Hydrogen Production from Formic Acid over Au Catalysts Supported on Carbon: Comparison with Au Catalysts Supported on SiO$_2$ and Al$_2$O$_3$

Dmitri A. Bulushev [1,*] **, Vladimir I. Sobolev** [1] **, Larisa V. Pirutko** [1] **, Anna V. Starostina** [1,2] **, Igor P. Asanov** [2,3] **, Evgenii Modin** [4] **, Andrey L. Chuvilin** [4,5] **, Neeraj Gupta** [6] **, Alexander V. Okotrub** [2,3] **and Lyubov G. Bulusheva** [2,3,*]

[1] Laboratory of Catalytic Methods of Solar Energy Transformation, Boreskov Institute of Catalysis, Russian Academy of Sciences, SB RAS, 630090 Novosibirsk, Russia; visobo@catalysis.ru (V.I.S.); pirutko@catalysis.ru (L.V.P.); khimik1@gmail.com (A.V.S.)

[2] Laboratory of Carbon Nanomaterials, Novosibirsk State University, 630090 Novosibirsk, Russia; asan@niic.nsc.ru (I.P.A.); spectrum@niic.nsc.ru (A.V.O.)

[3] Laboratory of Physico-Chemistry of Nanomaterials, Nikolaev Institute of Inorganic Chemistry, SB RAS, 630090 Novosibirsk, Russia

[4] CIC nanoGUNE Consolider, 20018 San Sebastian, Spain; e.modin@nanogune.eu (E.M.); a.chuvilin@nanogune.eu (A.L.C.)

[5] IKERBASQUE, Basque Foundation for Science, 20013 Bilbao, Spain

[6] Faculty of Basic Sciences, Shoolini University, Solan (HP) 173212, India; gupta_nrj@yahoo.co.in

[*] Correspondence: dmitri.bulushev@catalysis.ru (D.A.B.); bul@niic.nsc.ru (L.G.B.)

Abstract: Characteristics and catalytic activity in hydrogen production from formic acid of Au catalysts supported on porous N-free (Au/C) and N-doped carbon (Au/N-C) have been compared with those of Au/SiO$_2$ and Au/Al$_2$O$_3$ catalysts. Among the catalysts examined, the Au/N-C catalyst showed the highest Au mass-based catalytic activity. The following trend was found at 448 K: Au/N-C > Au/SiO$_2$ > Au/Al$_2$O$_3$, Au/C. The trend for the selectivity in hydrogen production was different: Au/C (99.5%) > Au/Al$_2$O$_3$ (98.0%) > Au/N-C (96.3%) > Au/SiO$_2$ (83.0%). According to XPS data the Au was present in metallic state in all catalysts after the reaction. TEM analysis revealed that the use of the N-C support allowed obtaining highly dispersed Au nanoparticles with a mean size of about 2 nm, which was close to those for the Au catalysts on the oxide supports. However, it was by a factor of 5 smaller than that for the Au/C catalyst. The difference in dispersion could explain the difference in the catalytic activity for the carbon-based catalysts. Additionally, the high activity of the Au/N-C catalyst could be related to the presence of pyridinic type nitrogen on the N-doped carbon surface, which activates the formic acid molecule forming pyridinium formate species further interacting with Au. This was confirmed by density functional theory (DFT) calculations. The results of this study may assist the development of novel Au catalysts for different catalytic reactions.

Keywords: formic acid; hydrogen production; gold; N-doped carbon; SiO$_2$; Al$_2$O$_3$

1. Introduction

Supported highly dispersed gold attracts a lot of attention as a catalyst—the properties of which could be better than those of the dispersed Pt-group metals. Scurrell [1] noted that gold recovery is to a large extent much easier than that of Pt-group metals. These factors can make the economics of using expensive gold rather than the Pt-group metals attractive. Carbon supports might provide some beneficial properties as compared to oxide supports like a very high surface area leading to a high

dispersion of metal, high inertness with respect to reactants, basic and acidic media, the presence of specific surface sites able to interact strongly with metals, and the possibility to regenerate easily an expensive metal by simply burning the support away [2–4]. Additionally, carbon supports could be obtained from carbon containing wastes and biomass. Nevertheless, carbon supported Au is relatively rarely studied. One of the reasons for this is the difficulty of synthesizing highly dispersed (<3 nm) gold nanoparticles with a narrow particle size distribution [4–10].

Formic acid is a liquid organic hydrogen carrier containing 4.4 wt% of hydrogen, which can be easily stored, transported, and used as compared to molecular hydrogen [11–13]. Low toxicity, high stability, low flammability, and biodegradability provide additional advantages for the utilization of formic acid as a hydrogen carrier. It is important that formic acid can be produced sustainably at low temperatures (<373 K) using catalysis from biomass [14,15] as well as by hydrogenation of carbon dioxide with hydrogen produced by electrolysis [16,17]. Hydrogen can be liberated from formic acid using supported metallic catalysts at mild conditions. Ojeda and Iglesia [18] reported that the activity of Au/Al_2O_3 catalysts for the gas-phase reaction was higher than that of Pt/Al_2O_3 catalysts. The activity of supported Au catalysts in formic acid decomposition depends on the type of the support [19,20], Au dispersion [18,21], and doping with alkali metal formates/carbonates [22,23].

The dispersed gold catalysts on carbon might be beneficial for the hydrogen production from formic acid decomposition taking into account the advantages of utilization of carbon support mentioned above. Earlier, some Au/C catalysts were tested in the gas-phase [20,24] and in liquid-phase [10] formic acid decomposition. The former experiments showed high selectivity for the hydrogen production, even at relatively high temperatures (≥473 K). Thus, it was significantly higher over an Au/C catalyst (about 95%) than that over an Au/TiO_2 catalyst (<70%) [24], where the TiO_2 support could participate in the reaction decreasing the selectivity through the conversion of formic acid into CO and H_2O.

It is important that carbon supports can be functionalized by the insertion of nitrogen [25–28], which may affect the gold dispersion and change the activity, selectivity, and stability of the catalyst. Despite gold supported on the N-doped carbon, carbon nitride has attracted the attention of researchers for its utilization as a catalyst for different reactions [9,29–31]. The effect of nitrogen on the catalytic performance of Au catalysts in formic acid decomposition is not known. Recently, we demonstrated that N-doping of carbon supports for Pd [32–34], Pt [35], Ru [35,36], and Cu [37] catalysts significantly promoted the gas-phase formic acid decomposition. The promotion was assigned to improving the metal dispersion for Cu [37] and appearance of novel active sites—single metal atoms of Pt-group metals stabilized by N-species of the support [32–35,38]. Liquid-phase formic acid decomposition over some Pd/C catalysts was also reported to be improved by N-doping of the carbon support [25,26,39,40]. Hence, we could expect that the promotional effect of nitrogen in the carbon support will also take place for this reaction over Au catalysts.

Therefore, we studied the effect of N-doping of the carbon support on the properties of Au catalysts in formic acid decomposition. We compared the catalytic performances of the Au catalysts supported on the N-doped and N-free carbon, SiO_2 and Al_2O_3 supports. Using high-angle annular dark field scanning transmission electron microscopy (HAADF/STEM) and X-ray photoelectron spectroscopy (XPS) we determined the Au particle size distributions and Au electronic state in the catalysts. Density functional theory (DFT) calculations allowed elucidation of the basic steps of the mechanism of the formic acid conversion on the Au/N-C catalyst.

2. Results and Discussion

2.1. Electron Microscopy Study

Table 1 shows the characteristics of the studied catalysts. It is seen that the content of gold was the same in all the samples (~2%) except of the Au/N-C sample (0.7%). The surface concentration of gold in the carbon supported catalysts was determined by XPS and a good correspondence with the bulk chemical analysis data was obtained. The smaller content of Au in the Au/N-C sample indicates that

the N-doped carbon support contains a smaller concentration of surface sites able to interact strongly with the Au precursor as compared to alumina and silica supports.

Table 1. Some characteristics and kinetic data for the supported Au catalysts.

	BET Surface Area of Support, $m^2 g^{-1}$	Au Bulk Content, wt%	Au Surface Content,[3] wt% (XPS)	Au $f_{7/2}$ (FWHM),[3] eV (XPS)	Mean Particle Size,[3] nm (TEM)	Reaction Rate at 448 K,[4] s^{-1}	E_a, kJ mol^{-1}	Selectivity to H_2 at 448 K, %
Au/C	873	1.9[1]	1.8	84.1 (0.9)	10 ± 6	0.019	58	99.5
Au/N-C	674	0.7[1]	0.8	83.9 (1.48)	2.2 ± 0.9	0.045	53	96.6
Au/Al$_2$O$_3$	200	1.8[2]	1.5	83.9 (2.13)	2.2 ± 1.0	0.017	48	98.0
Au/SiO$_2$	480	2.1[2]	0.4	84.1 (2.22)	1.6 ± 0.8	0.032	63	83.0

[1] Determined by atomic-absorption spectroscopy (AAS). [2] Determined by inductively coupled plasma optical emission spectroscopy (ICPOES). [3] Determined after the reaction. [4] Related to the total number of Au atoms in the catalyst.

The mean Au particle size determined from low magnification images was relatively high for the Au/C catalyst (~10 nm, Figure 1a). However, for the Au/N-C (Figure 2a) and Au/Al$_2$O$_3$ (Figure 3) catalysts it was low and corresponded to 2.2 nm. For the Au/SiO$_2$ catalyst, it was by a factor of 1.4 lower (1.6 nm, Figure 3). Hence, the N-C support demonstrated the Au dispersion similar to those for the oxides, but not to that for the N-free carbon support.
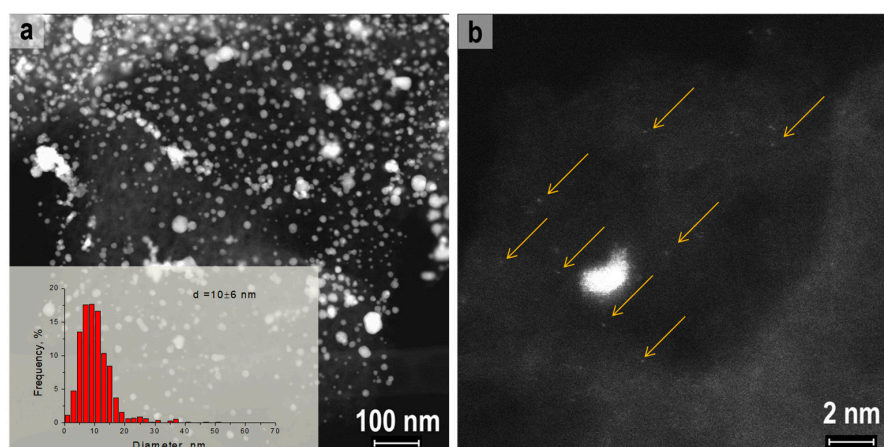

Figure 1. (**a**) Low- and (**b**) high-magnification HAADF/STEM images of the 1.9% Au/C sample after the reaction. The insert shows Au particle size distribution. (**b**) Some single Au atoms are indicated by arrows.
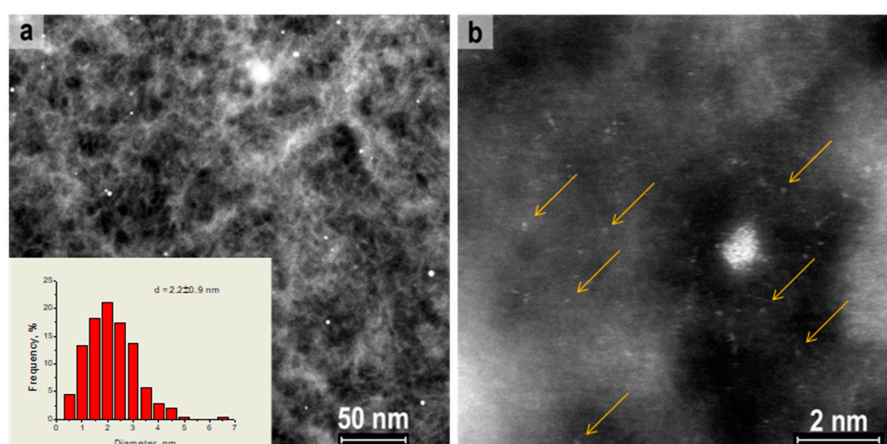

Figure 2. (**a**) Low- and (**b**) high-magnification HAADF/STEM images of the 0.7% Au/N-C sample after the reaction. The insert shows Au particle size distribution. (**b**) Some single Au atoms are indicated by arrows.
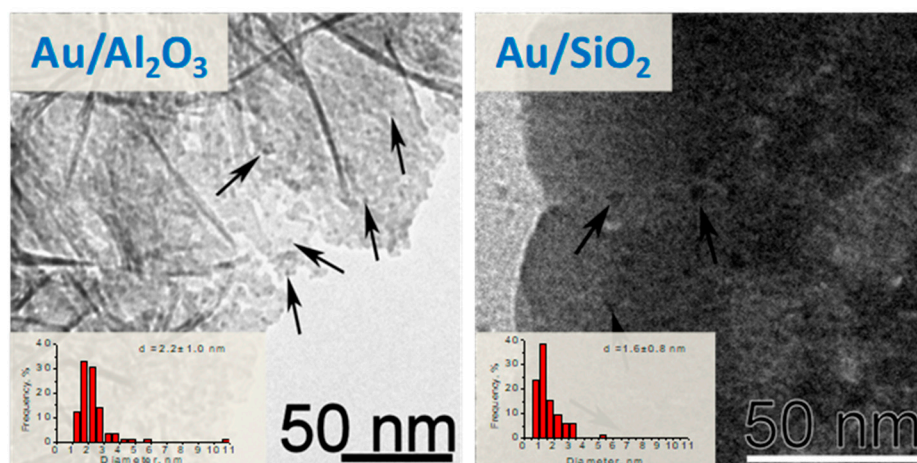
Figure 3. TEM images and particle size distributions for the Au/Al$_2$O$_3$ and Au/SiO$_2$ catalysts after the reaction. Some Au particles are indicated by arrows.

Using a higher magnification, single Au atoms and few-atoms clusters are seen in HAADF/STEM images of the Au/C catalyst (Figure 1b) and of the Au/N-C catalyst (Figure 2b). For the latter sample, the contribution of these Au species could be even higher due to a higher overall dispersion of Au. It is important that the single atoms are not stabilized by chlorine as no chlorine was found in the samples by XPS [41]. Hence, gold in the both carbon supported catalysts is presented as single metal atoms and nanoparticles. These particles are of about 2 nm sizes for the N-doped carbon, SiO$_2$ and Al$_2$O$_3$, and about 10 nm for the N-free sample (Table 1, Figures 1–3). Thus, N-doping of the carbon support led to a significant improvement of the Au dispersion.

2.2. XPS Study

Synchrotron radiation based N 1s XPS spectrum of the Au/N-C sample is presented in Figure 4. The spectrum was fitted by four components corresponding to pyridinic N (398.3 eV, 30 at%), pyrrolic N (400.0 eV, 49 at%), graphitic N (401.0 eV, 15 at%), and pyridine-N-oxide (402.8 eV, 6 at%) states. The total surface content of nitrogen in the sample was 4.6 at%. No nitrogen was found in the Au/C sample.
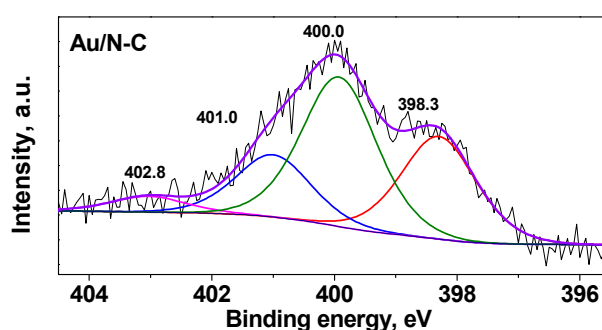

Figure 4. Synchrotron radiation based XPS N 1s spectrum of the 0.7% Au/N-C catalyst after the reaction.

The Au catalysts after the reaction were studied by a laboratory XPS to understand the electronic state of Au. These studies showed the presence of Au only in metallic state (Au 4f$_{7/2}$~84.0 eV) (Figure 5). The position of the Au 4f$_{7/2}$ peaks for all the catalysts was the same within experimental error (±0.1 eV). Much narrower Au 4f$_{7/2}$ lines for the Au/C catalyst as compared to other catalysts should be assigned to a much bigger size of the metallic Au nanoparticles in this sample (Table 1) in accordance with the data in the literature [42]. The presence of chlorine atoms was not found in the samples.
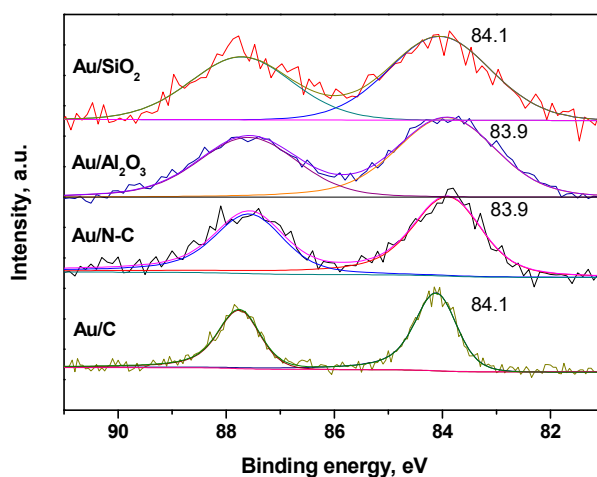
Figure 5. XPS spectra of the Au 4f region of the studied catalysts after the reaction.

Single Au atoms as well as single Pt-group metals atoms are known to be present in a cationic state and not in a metallic state on different supports [9,32,34,35,38,43–46]. Single Au atoms observed by HAADF/STEM (Figures 1 and 2) either present in a small concentration, or present initially in a cationic state but can be photo-reduced during the XPS measurements [44].

Therefore, the support nature does not affect noticeably the electronic state of Au. The state of Au after the reaction in all the catalysts is metallic. Nitrogen is present in different forms in the N-doped catalyst.

2.3. Catalytic Activity

The conversion-temperature curves for the carbon supported Au catalysts and the N-C support are shown in Figure S1. The N-C support was studied because N-C materials may participate in some catalytic reactions in the absence of supported metal [47–49]. However, in our case the activity of the N-C material was by a factor of 10 lower than that of the Au containing materials. The conversion curves for the Au/C and Au/N-C catalysts are almost similar despite a significantly smaller content of Au in the N-doped sample (Table 1). This indicates that the reaction rate based on the Au mass is significantly higher for the N-doped catalyst (Table 1). This result could be provided by a higher Au dispersion in this catalyst. Ojeda and Iglesia [18] as well as Singh et al. [21] showed that the reaction rate increases with a decrease of the Au mean particle size for the Au catalysts supported on alumina and silicon carbide, respectively. The former authors supposed that the content of active sub-nanometric Au species increases with an increase of the dispersion, while the latter authors supposed that low-coordinated Au sites present in nanoparticles are the active sites of the reaction and their content increases with an increase of the dispersion.

The conversion—temperature curves for the oxide supported Au catalysts are compared in Figure S2. The conversion of formic acid over the SiO_2 supported catalyst is higher than that over the Al_2O_3 supported catalyst. Lower sample charges to the reactor were used for these catalysts as compared to the carbon supported samples (Figure S1). Hence, the reaction rates determined per the total content of Au atoms have been calculated for all four samples and the following trend of the activity was obtained: Au/N-C > Au/SiO_2 > Au/C, Au/Al_2O_3 (Table 1, Figure 6). Thus, the reaction rate for the Au/N-C catalyst at 448 K was by a factor of 2.5 higher than that for the Au/C and Au/Al_2O_3 samples. This difference is clearly seen in Figure 6 representing the Arrhenius plots. The rates per the number of surface sites (turnover frequencies) were not calculated, as a contribution of single Au atoms to the content of Au in the samples is not known and cannot be estimated using, for example, CO adsorption like in the case of supported Pt-group metals [33,35].
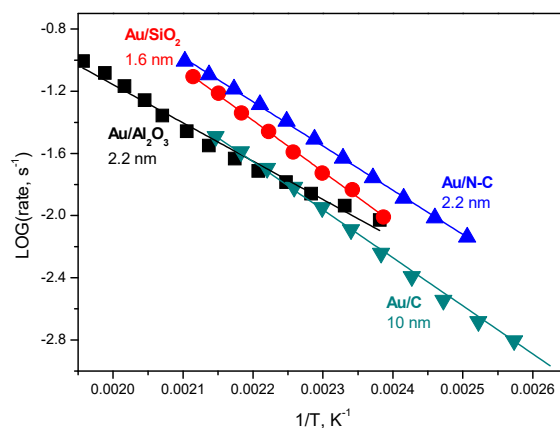
Figure 6. Arrhenius plots for formic acid decomposition over the studied Au catalysts on different supports. The mean Au particle sizes are indicated.

The apparent activation energies (E_a) for the studied Au catalysts are in the range from 48 up to 63 kJ mol^{-1} (Table 1). These values correspond well to the literature values for different supported Au catalysts [18,19,21,24]. Earlier, we showed that the alumina supported Au catalysts were more active than the Au catalysts supported on amphoteric and basic supports like ZrO_2, CeO_2, La_2O_3, and MgO oxides [19]. However, the present study indicated that the activity of the Au/Al_2O_3 catalyst was lower than that of the Au catalysts supported on the N-C and SiO_2 supports despite the lowest apparent activation energy for this catalyst (48 kJ mol^{-1}, Table 1). These data probably show that a smaller ratio of the surface Au atoms is active in this sample than in the other samples. These could be low coordinated Au or Au-support interface sites the concentration of which could depend on the particle size and particle shape determined by the support nature.

The selectivity for the hydrogen production from formic acid at 448 K is shown in Table 1. The Au/C catalyst demonstrated the best selectivity (99.5%) implying almost complete conversion of formic acid into H_2 and CO_2. The Au/N-C and Au/Al_2O_3 catalysts showed slightly lower selectivities of 96.6 and 98%, respectively; while the selectivity over the Au/SiO_2 catalyst was the lowest (83%). The low selectivity for the latter catalyst may indicate that in this catalyst there is a higher ratio of the sites able to convert formic acid not into CO_2 and H_2, but into CO and H_2O.

The presented data confirmed that the catalyst support strongly affects the catalytic performance of the Au catalysts despite the electronic state of Au in the studied samples determined by XPS being the same and corresponding to metallic Au (Figure 5). The Au/N-C catalyst showed a higher hydrogen yield from decomposition of formic acid as compared to the Au catalysts supported on the N-free carbon, alumina or silica. Additionally, the gold in the N-doped Au sample could be used more efficiently for catalysis than that in the Au/C sample as the dispersion of Au is higher (53% and 12%, respectively).

Earlier, different research groups proposed that sub-nanometer Au clusters [18,50,51] or single Au atoms [45] supported on some oxide supports (CeO_2 [45,50], ZrO_2 [51] and Al_2O_3 [18]) are the active sites in formic acid decomposition. Hutchings et al. [43,44] showed that single Au cations stabilized by chlorine on carbon supports are the active sites for acetylene hydrochlorination. Lin et al. [9] demonstrated that single Au atoms in N-doped carbon can be efficient in semi-hydrogenation of different alkynes. Single Au atoms and small Au clusters were observed in our carbon supported samples in the absence of chlorine by HAADF/STEM (Figures 1b and 2b). It is an interesting question whether they can be the key active sites for the reaction. Recently, we have considered interaction of the formic acid molecule with the single Au atoms attached to different positions of the N-doped graphene fragment using DFT calculations [41]. In contrast to the single atoms of the Pt-group metals which are able to break the bonds in the incoming formic acid molecule [32,33,35], the single Au atoms were found to coordinate the molecule through the oxygen atom. In the present study, using DFT

calculations, we have considered the interaction of the formic acid molecule through the hydrogen atom directed to the pyridinic atom located near the Au atom (Figure S3).

2.4. DFT Calculations

The DFT calculations have been performed with a goal to understand whether nitrogen species in the support can activate the formic acid molecule for interaction with Au species. Our calculations showed no adsorption of the formic acid molecule at the graphitic and pyrrolic N species. The molecule moved away from these N species during the optimization process. However, the molecule was stabilized at the edge pyridinic N atom via the hydrogen atom of the hydroxyl group (Figure 7). The binding energy between the molecule and the N-graphene fragment was relatively strong (0.81 eV). The N···H(O) distance was small (1.50 Å) indicating the formation of the bond. The calculated length of the O-H bond in the free formic acid molecule is 0.965 Å and this length increased to 0.989 Å when the molecule was adsorbed. From the literature, it is known that a relatively stable, up to 386 K, pyridinium formate ($[C_5H_6N^+][HCOO^-]$) could be formed by a reaction of formic acid and pyridine [52]. We suppose the breaking of the O-H bond at elevated temperature with protonation of the pyridinic nitrogen atom and formation of the formate species with a structure similar to that of pyridinium formate. In this way, the N-C support may activate the formic acid molecule.
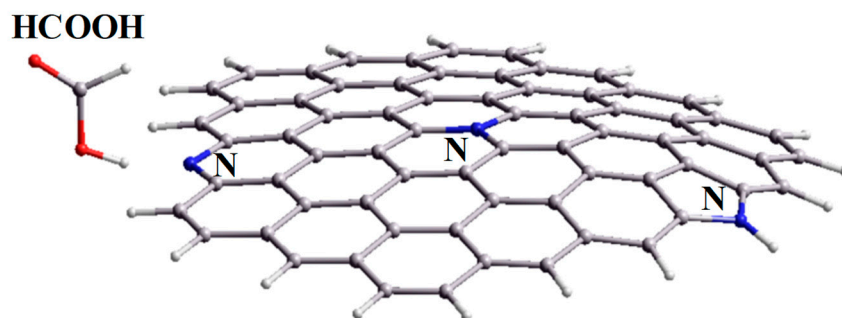

Figure 7. Optimized position of the formic acid molecule with respect to the N-doped graphene fragment.

Optimization of the geometry of the formic acid molecule and the catalyst fragment (Au at N-graphene fragment, Figure 8a) also found a local energy minimum corresponding to adsorption of the molecule at the pyridinic nitrogen atom located near the Au atom on the edge of the fragment. In the optimized position, the N···H(O) distance was equal to 1.76 Å. In this case the protonation of the pyridinic N atom takes place as well as for the N-doped fragment without the Au atom (Figure 7). The binding energy of the molecule with this fragment was stronger than that with the fragment without Au and equal to 0.88 eV. This value was also higher than the value in the case when the formic acid molecule was adsorbed through the oxygen atom of the OH group directly on the Au atom in a similar configuration (0.72 eV) [41].

Therefore, at elevated temperatures, the interaction of the formic acid molecule with the pyridinic N atom results in the rupture of the O-H bond accompanied by attachment of the released hydrogen atom to nitrogen. Interaction of the formate species with a fragment containing the protonated pyridinic nitrogen atom and the Au atom present nearby was also considered (Figure 8b). The results indicated that the oxygen atom of the formate species may form a hydrogen bond with the hydrogen atom of the protonated nitrogen atom. The energy gain obtained due to the reconstruction of the structure depicted in Figure 8a into the structure with the adsorbed formate (Figure 8b) is equal to 1.20 eV. The calculated distance between the oxygen atom in the formate species and the hydrogen atom of the protonated pyridinic N atom is equal to 1.93 Å. Therefore, the interaction of the formic acid with the pyridinic nitrogen atom leads to its protonation and formation of the formate species.

Moreover, the calculations showed that the formate species can be further converted to adsorbed hydrogen species and gaseous CO_2. The energy determining step in the formation of the CO_2 molecule

could be decomposition of the formate species at the single Au atom accompanied by the formation of the Au-H bond (1.65 Å) (Figure 8c). The energy of such a structure is only by 0.46 eV higher than the total energy calculated for the structure shown in Figure 8b indicating the possibility of this reaction. Schmidbaur et al. [53] reported the Au-H bond lengths in the range from 1.542 to 1.706 Å for different Au hydrides and Au hydride complexes in accordance with the results obtained in this study.
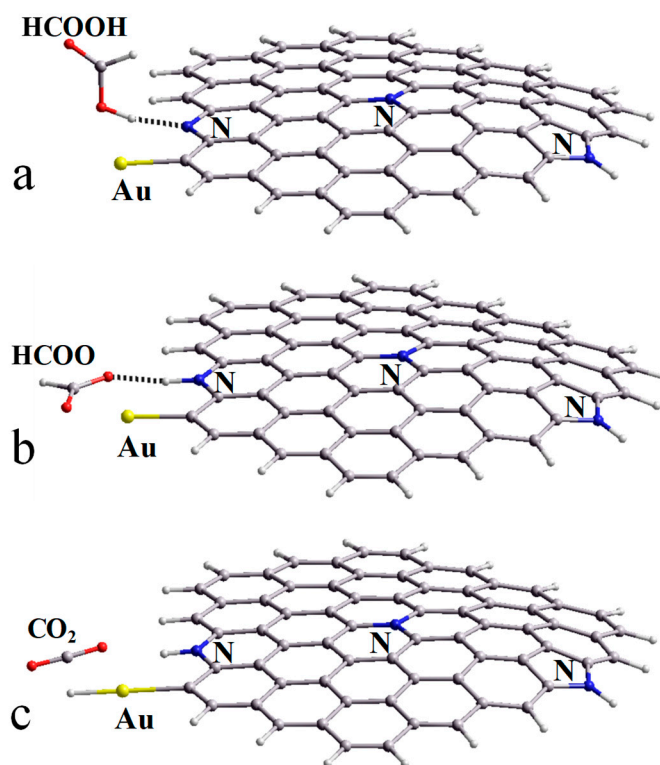

Figure 8. (**a**) Interaction of the formic acid molecule with the Au containing N-doped graphene fragment, (**b**) interaction of the formate species with the protonated pyridinic nitrogen atom located near the Au atom and (**c**) decomposition of the formate species.

Hence, the pyridinic nitrogen atom present near the single Au atom can play an important role in the formic acid molecule conversion to the CO_2 and H_2 products. This reaction occurs through the protonation of the pyridinic N atom and formation of the formate species, which further converts on the single Au atom to gaseous CO_2 and the hydrogen atom adsorbed on that Au atom. The following reaction steps probably take place:

$$>N + HCOOH \rightarrow >NH^+HCOO^-$$
$$>NH^+HCOO^- + Au \rightarrow >NH + AuH + CO_2$$
$$>NH + AuH \rightarrow >N + Au + H_2.$$
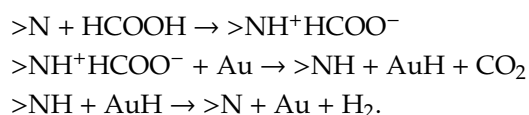
Yet, more evidence is needed for the third step.

A similar mechanism can be valid also for Au clusters located near the pyridinic nitrogen species. This mechanism could provide a benefit in the activity of the Au/N-C catalyst as compared to other Au catalysts containing Au nanoparticles of the same mean particle size (Figure 6).

3. Materials and Methods

3.1. Materials

Commercial SiO_2 (Merck) and Al_2O_3 (A-201 La Roche Industries Inc., Baton Rouge, LA, USA) have been used as oxide supports. N-free and N-doped porous carbon materials were synthesized

by chemical vapor deposition from ethanol at 1073 K and acetonitrile at 973 K, respectively, using the product of thermolysis of iron-doped (1.4 wt%) calcium tartrate as a template, as is described earlier [32,33,54]. Both carbon supports were mesoporous [32]. The Brunauer-Emmett-Teller (BET) surface areas of all the catalyst supports used are shown in Table 1.

Gold was deposited on the oxide supports by an adsorption method using a procedure described by Ivanova et al. [55]. A water solution of $HAuCl_4$ (99.9%, ABCR, Darmstadt, Germany) with a concentration of 5×10^{-4} M was mixed with a support in a ratio corresponding to the Au concentration of 2 wt%. After stirring at 343 K for 2 h, a 4 M solution of ammonia was added. The suspension was stirred again for 1 h at 343 K, then filtered and washed in water. The samples were dried for a night at 353 K and calcined at 573 K for 4 h.

Gold was deposited on the carbon supports using a similar method. Thus, the carbon support was placed into a water solution of $HAuCl_4$. After interaction for 1 h at 343 K, the precipitate was separated by centrifugation and placed into a 10 wt% NH_3-water solution at 333 K for 1 h. The obtained precipitate was washed with water, centrifuged, and dried in air at room temperature and then for a night at 353 K.

3.2. Characterization

X-ray photoelectron spectroscopy (XPS) measurements of the samples were performed on a SPECS Phoibos 150 (Berlin, Germany) laboratory spectrometer using a monochromatized AlKα radiation (1486.6 eV). A carbon C 1s peak for hydrocarbon impurities at 285.0 eV was used as a reference for the energy scale calibration.

The fine N 1s lines of the samples were recorded at the Berliner Elektronen-Speicherring für Synchrotronstrahlung (BESSY) using radiation from the Russian-German beamline. The spectra were measured at the energy of monochromatized synchrotron radiation of 830 eV. In this case, the binding energies were calibrated to the Au $4f_{7/2}$ line from a gold foil peaked at 84.0 eV.

To determine the particle size distributions, the samples were studied using a conventional transmission electron microscope Zeiss LEO 912 OMEGA (Freiburg, Germany) at acceleration voltage of 120 kV and a FEI Titan 60–300 (Eindhoven, The Netherlands) microscope at acceleration voltage of 300 kV in HAADF/STEM mode. At least 100 metal particles have been measured for particle size distribution analysis.

3.3. Catalytic Measurements

Gas-phase formic acid decomposition was carried out in a fixed-bed tubular glass reactor. Activity tests were performed at atmospheric pressure with 20 or 50 mg of a catalyst. All catalysts were pretreated in a flow of 5 vol% formic acid in He (20 cm^3 min^{-1}) while heating with a ramp rate of 2 K min^{-1} up to 573 K, keeping for 15 min at this temperature and cooling in the same mixture to the reaction temperature (first heating cycle). A second heating cycle was performed in order to get a temperature dependence of the formic acid conversion for comparison of the catalytic activity of the samples.

The components of the reaction mixture were analyzed by gas chromatography as described earlier [37]. The reaction rates and apparent activation energies were calculated at low conversions (<25%).

3.4. DFT Calculations

Theoretical modeling was carried out using the hybrid functional M06, parameterized for metal-organic systems [56], with inclusion of a dispersion correction developed by Grimme et al. [57,58] (M06-D3 method). The calculations were carried out within the quantum-chemical program package Jaguar (Jaguar, version 9.8, Schrödinger, LLC, New York, NY, USA, 2017). A set of LACVP** basis functions with polarization functions on all elements except for Au was used.

An N-doped carbon substrate was presented by a nitrogen-containing graphene fragment $C_{69}N_3H_{13}$ with hydrogen-terminated edges (Figure S3). Based on XPS data, three types of nitrogen defects were inserted in the fragment: Three-coordinated graphitic N in the center of the fragment (1), two-coordinated pyridinic N (2), and three-coordinated pyrrolic N (3).

A catalyst substrate with a gold atom substituting hydrogen atom near the pyridinic N atom was presented by a fragment shown in Figure S3. This model was constructed based on our previous DFT studies, which showed that an Au atom does not like pyridinic N at the graphene edge and prefers to attach to the neighboring naked carbon atom [41].

The binding energy of the formic acid molecule with the Au containing N-doped graphene fragment was calculated as: $E_{bin} = E_{tot}(fragment) + E_{tot}(FA) − E_{tot}(model)$, where $E_{tot}(fragment)$, $E_{tot}(FA)$ and $E_{tot}(model)$ are the total energy of the graphene fragment, the energy of the formic acid molecule, and the energy of the model, respectively.

4. Conclusions

The present work showed that the nature of the support (C, N-C, SiO_2, Al_2O_3) does not affect the electronic state of supported Au nanoparticles present in the metallic state. At the same time, a significant effect of the support for the hydrogen production from formic acid decomposition was found. The Au/N-C catalyst showed a higher hydrogen yield than those for the Au/C, Au/SiO_2, and Au/Al_2O_3 catalysts. For the Au/N-C sample, interaction of the formic acid molecule takes place with the basic pyridinic nitrogen atom transforming it to the protonated state and simultaneous formation of the formate species. The breakage of the C-H bond in the formate species on the single Au atom as compared to the breakage of the bonds in the formic acid molecule takes place more easily, explaining the high activity of the Au/N-C catalyst in the reaction. The results of this paper could be used for the development of highly dispersed Au catalysts for different valuable reactions including energy related reactions.

Supplementary Materials: The following are available online at http://www.mdpi.com/2073-4344/9/4/376/s1, Figure S1: Comparison of the conversion–temperature curves for formic acid decomposition over the N-doped, N-free Au catalysts and N-doped carbon support, Figure S2: Comparison of the conversion–temperature curves for formic acid decomposition over Au catalysts supported on SiO_2 and Al_2O_3, Figure S3: Initial N-graphene and Au-N-graphene fragments used for DFT calculations.

Author Contributions: Data analysis, writing, D.A.B.; synthesis and catalytic measurements, V.I.S., L.V.P., A.V.S. and N.G.; electron microscopy measurements, A.L.C. and E.M.; XPS measurements, I.P.A. and A.V.O.; quantum chemical calculations, writing, L.G.B.

Conflicts of Interest: The authors declare no conflict of interest.

References

1. Scurrell, M.S. Thoughts on the Use of Gold-Based Catalysts in Environmental Protection Catalysis. *Gold Bull.* **2017**, *50*, 77–84. [CrossRef]
2. Prati, L.; Villa, A.; Lupini, A.R.; Veith, G.M. Gold on Carbon: One Billion Catalysts under a Single Label. *Phys. Chem. Chem. Phys.* **2012**, *14*, 2969–2978. [CrossRef]
3. Rodríguez-Reinoso, F. The Role of Carbon Materials in Heterogeneous Catalysis. *Carbon* **1998**, *36*, 159–175. [CrossRef]
4. Bulushev, D.A.; Yuranov, I.; Suvorova, E.I.; Buffat, P.A.; Kiwi-Minsker, L. Highly Dispersed Gold on Activated Carbon Fibers for Low-Temperature CO Oxidation. *J. Catal.* **2004**, *224*, 8–17. [CrossRef]
5. Pyryaev, P.A.; Moroz, B.L.; Zyuzin, D.A.; Nartova, A.V.; Bukhtiyarov, V.I. Nanosized Au/C Catalyst Obtained from a Tetraamminegold(III) Precursor: Synthesis, Characterization, and Catalytic Activity in Low-Temperature CO Oxidation. *Kinet. Catal.* **2010**, *51*, 885–892. [CrossRef]

6. Megias-Sayago, C.; Santos, J.L.; Ammari, F.; Chenouf, M.; Ivanova, S.; Centeno, M.A.; Odriozola, J.A. Influence of Gold Particle Size in Au/C Catalysts for Base-Free Oxidation of Glucose. *Catal. Today* **2018**, *306*, 183–190. [CrossRef]

7. Yushchenko, D.Y.; Simonov, P.A.; Khlebnikova, T.B.; Pai, Z.P.; Bukhtiyarov, V.I. Oxidation of N-Isopropyl Phosphonomethyl Glycine with Hydrogen Peroxide Catalyzed by Carbon-Supported Gold Nanoparticles. *Catal. Commun.* **2019**, *121*, 57–61. [CrossRef]

8. Liotta, L.F. New Trends in Gold Catalysts. *Catalysts* **2014**, *4*, 299–304. [CrossRef]

9. Lin, R.; Albani, D.; Fako, E.; Kaiser, S.K.; Safonova, O.V.; López, N.; Pérez-Ramírez, J. Design of Single Gold Atoms on Nitrogen-Doped Carbon for Molecular Recognition in Alkyne Semi-Hydrogenation. *Angew. Chem. Int. Ed.* **2019**, *58*, 504–509. [CrossRef]

10. Grad, O.; Mihet, M.; Dan, M.; Blanita, G.; Radu, T.; Berghian-Grosan, C.; Lazar, M.D. Au/Reduced Graphene Oxide Composites: Eco-Friendly Preparation Method and Catalytic Applications for Formic Acid Dehydrogenation. *J. Mater. Sci.* **2019**, *54*, 6991–7004. [CrossRef]

11. Gianotti, E.; Taillades-Jacquin, M.; Roziere, J.; Jones, D.J. High-Purity Hydrogen Generation Via Dehydrogenation of Organic Carriers: A Review on the Catalytic Process. *ACS Catal.* **2018**, *8*, 4660–4680. [CrossRef]

12. Niermann, M.; Beckendorff, A.; Kaltschmitt, M.; Bonhoff, K. Liquid Organic Hydrogen Carrier (LOHC)—Assessment Based on Chemical and Economic Properties. *Int. J. Hydrog. Energy* **2019**, *44*, 6631–6654. [CrossRef]

13. Zhong, H.; Iguchi, M.; Chatterjee, M.; Himeda, Y.; Xu, Q.; Kawanami, H. Formic Acid-Based Liquid Organic Hydrogen Carrier System with Heterogeneous Catalysts. *Adv. Sustain. Syst.* **2018**, *2*, 1700161. [CrossRef]

14. Bulushev, D.A.; Ross, J.R.H. Towards Sustainable Production of Formic Acid. *ChemSusChem* **2018**, *11*, 821–836. [CrossRef]

15. Preuster, P.; Albert, J. Biogenic Formic Acid as a Green Hydrogen Carrier. *Energy Technol.* **2018**, *6*, 501–509. [CrossRef]

16. Bulushev, D.A.; Ross, J.R.H. Heterogeneous Catalysts for Hydrogenation of CO_2 and Bicarbonates to Formic Acid and Formates. *Catal. Rev.* **2018**, *60*, 566–593. [CrossRef]

17. Wang, W.H.; Himeda, Y.; Muckerman, J.T.; Manbeck, G.F.; Fujita, E. CO_2 Hydrogenation to Formate and Methanol as an Alternative to Photo- and Electrochemical CO_2 Reduction. *Chem. Rev.* **2015**, *115*, 12936–12973. [CrossRef]

18. Ojeda, M.; Iglesia, E. Formic Acid Dehydrogenation on Au-Based Catalysts at near-Ambient Temperatures. *Angew. Chem. Int. Ed.* **2009**, *48*, 4800–4803. [CrossRef]

19. Zacharska, M.; Chuvilin, A.L.; Kriventsov, V.V.; Beloshapkin, S.; Estrada, M.; Simakov, A.; Bulushev, D.A. Support Effect for Nanosized Au Catalysts in Hydrogen Production from Formic Acid Decomposition. *Catal. Sci. Technol.* **2016**, *6*, 6853–6860. [CrossRef]

20. Gazsi, A.; Bansagi, T.; Solymosi, F. Decomposition and Reforming of Formic Acid on Supported Au Catalysts: Production of CO-Free H2. *J. Phys. Chem. C* **2011**, *115*, 15459–15466. [CrossRef]

21. Singh, S.; Li, S.; Carrasquillo-Flores, R.; Alba-Rubio, A.C.; Dumesic, J.A.; Mavrikakis, M. Formic Acid Decomposition on Au Catalysts: DFT, Microkinetic Modeling, and Reaction Kinetics Experiments. *AIChE J.* **2014**, *60*, 1303–1319. [CrossRef]

22. Bulushev, D.A.; Zacharska, M.; Guo, Y.; Beloshapkin, S.; Simakov, A. CO-Free Hydrogen Production from Decomposition of Formic Acid over Au/Al$_2$O$_3$ Catalysts Doped with Potassium Ions. *Catal. Commun.* **2017**, *92*, 86–89. [CrossRef]

23. Jia, L.; Bulushev, D.A.; Beloshapkin, S.; Ross, J.R.H. Hydrogen Production from Formic Acid Vapour over a Pd/C Catalyst Promoted by Potassium Salts: Evidence for Participation of Buffer-Like Solution in the Pores of the Catalyst. *Appl. Catal. B Environ.* **2014**, *160*, 35–43. [CrossRef]

24. Bulushev, D.A.; Beloshapkin, S.; Ross, J.R.H. Hydrogen from Formic Acid Decomposition over Pd and Au Catalysts. *Catal. Today* **2010**, *154*, 7–12. [CrossRef]

25. Cao, Y.; Mao, S.; Li, M.; Chen, Y.; Wang, Y. Metal/Porous Carbon Composites for Heterogeneous Catalysis: Old Catalysts with Improved Performance Promoted by N-Doping. *ACS Catal.* **2017**, *7*, 8090–8112. [CrossRef]

26. Salinas-Torres, D.; Navlani-García, M.; Mori, K.; Kuwahara, Y.; Yamashita, H. Nitrogen-Doped Carbon Materials as a Promising Platform toward the Efficient Catalysis for Hydrogen Generation. *Appl. Catal. A Gen.* **2019**, *571*, 25–41. [CrossRef]

27. Kudashov, A.G.; Okotrub, A.V.; Yudanov, N.F.; Romanenko, A.I.; Bulusheva, L.G.; Abrosimov, O.G.; Chuvilin, A.L.; Pazhetov, E.M.; Boronin, A.I. Gas-Phase Synthesis of Nitrogen-Containing Carbon Nanotubes and Their Electronic Properties. *Phys. Solid State* **2002**, *44*, 652–655. [CrossRef]

28. Podyacheva, O.Y.; Ismagilov, Z.R. Nitrogen-Doped Carbon Nanomaterials: To the Mechanism of Growth, Electrical Conductivity and Application in Catalysis. *Catal. Today* **2015**, *249*, 12–22. [CrossRef]

29. Zhao, J.; Xu, J.; Xu, J.; Zhang, T.; Di, X.; Ni, J.; Li, X. Enhancement of Au/AC Acetylene Hydrochlorination Catalyst Activity and Stability Via Nitrogen-Modified Activated Carbon Support. *Chem. Eng. J.* **2015**, *262*, 1152–1160. [CrossRef]

30. Gil, S.; Lucas, P.J.; Nieto-Márquez, A.; Sánchez-Silva, L.; Giroir-Fendler, A.; Romero, A.; Valverde, J.L. Synthesis and Characterization of Nitrogen-Doped Carbon Nanospheres Decorated with Au Nanoparticles for the Liquid-Phase Oxidation of Glycerol. *Ind. Eng. Chem. Res.* **2014**, *53*, 16696–16706. [CrossRef]

31. Dai, B.; Li, X.; Zhang, J.; Yu, F.; Zhu, M. Application of Mesoporous Carbon Nitride as a Support for an Au Catalyst for Acetylene Hydrochlorination. *Chem. Eng. Sci.* **2015**, *135*, 472–478. [CrossRef]

32. Bulushev, D.A.; Zacharska, M.; Shlyakhova, E.V.; Chuvilin, A.L.; Guo, Y.; Beloshapkin, S.; Okotrub, A.V.; Bulusheva, L.G. Single Isolated Pd2+ Cations Supported on N-Doped Carbon as Active Sites for Hydrogen Production from Formic Acid Decomposition. *ACS Catal.* **2016**, *6*, 681–691. [CrossRef]

33. Zacharska, M.; Bulusheva, L.G.; Lisitsyn, A.S.; Beloshapkin, S.; Guo, Y.; Chuvilin, A.L.; Shlyakhova, E.V.; Podyacheva, O.Y.; Leahy, J.J.; Okotrub, A.V.; et al. Factors Influencing the Performance of Pd/C Catalysts in the Green Production of Hydrogen from Formic Acid. *ChemSusChem* **2017**, *10*, 720–730. [CrossRef] [PubMed]

34. Podyacheva, O.Y.; Bulushev, D.A.; Suboch, A.N.; Svintsitskiy, D.A.; Lisitsyn, A.S.; Modin, E.; Chuvilin, A.; Gerasimov, E.Y.; Sobolev, V.I.; Parmon, V.N. Highly Stable Single-Atom Catalyst with Ionic Pd Active Sites Supported on N-Doped Carbon Nanotubes for Formic Acid Decomposition. *ChemSusChem* **2018**, *11*, 3724–3727. [CrossRef]

35. Bulushev, D.A.; Zacharska, M.; Lisitsyn, A.S.; Podyacheva, O.Y.; Hage, F.S.; Ramasse, Q.M.; Bangert, U.; Bulusheva, L.G. Single Atoms of Pt-Group Metals Stabilized by N-Doped Carbon Nanofibers for Efficient Hydrogen Production from Formic Acid. *ACS Catal.* **2016**, *6*, 3442–3451. [CrossRef]

36. Zacharska, M.; Podyacheva, O.Y.; Kibis, L.S.; Boronin, A.I.; Senkovskiy, B.V.; Gerasimov, E.Y.; Taran, O.P.; Ayusheev, A.B.; Parmon, V.N.; Leahy, J.J.; et al. Ruthenium Clusters on Carbon Nanofibers for Formic Acid Decomposition: Effect of Doping the Support with Nitrogen. *ChemCatChem* **2015**, *7*, 2910–2917. [CrossRef]

37. Bulushev, D.A.; Chuvilin, A.L.; Sobolev, V.I.; Stolyarova, S.G.; Shubin, Y.V.; Asanov, I.P.; Ishchenko, A.V.; Magnani, G.; Ricco, M.; Okotrub, A.V.; et al. Copper on Carbon Materials: Stabilization by Nitrogen Doping. *J. Mater. Chem. A* **2017**, *5*, 10574–10583. [CrossRef]

38. Chesnokov, V.V.; Kriventsov, V.V.; Malykhin, S.E.; Svintsitskiy, D.A.; Podyacheva, O.Y.; Lisitsyn, A.S.; Richards, R.M. Nature of Active Palladium Sites on Nitrogen Doped Carbon Nanofibers in Selective Hydrogenation of Acetylene. *Diam. Relat. Mater.* **2018**, *89*, 67–73. [CrossRef]

39. Bi, Q.Y.; Lin, J.D.; Liu, Y.M.; He, H.Y.; Huang, F.Q.; Cao, Y. Dehydrogenation of Formic Acid at Room Temperature: Boosting Palladium Nanoparticle Efficiency by Coupling with Pyridinic-Nitrogen-Doped Carbon. *Angew. Chem. Int. Ed.* **2016**, *55*, 11849–11853. [CrossRef]

40. Li, Z.P.; Yang, X.C.; Tsumori, N.; Liu, Z.; Himeda, Y.; Autrey, T.; Xu, Q. Tandem Nitrogen Functionalization of Porous Carbon: Toward Immobilizing Highly Active Palladium Nanoclusters for Dehydrogenation of Formic Acid. *ACS Catal.* **2017**, *7*, 2720–2724. [CrossRef]

41. Bulushev, D.A.; Chuvilin, A.L.; Sobolev, V.I.; Pirutko, L.V.; Fedoseeva, Y.V.; Lobiak, E.V.; Modin, E.; Okotrub, A.V.; Bulusheva, L.G. Single Au Atoms on the Surface of N-Free and N-Doped Carbon: Interaction with Formic Acid and Methanol Molecules. *Top. Catal.* **2019**, in press.

42. Peters, S.; Peredkov, S.; Neeb, M.; Eberhardt, W.; Al-Hada, M. Size-Dependent XPS Spectra of Small Supported Au-Clusters. *Surf. Sci.* **2013**, *608*, 129–134. [CrossRef]

43. Liu, X.; Conte, M.; Elias, D.; Lu, L.; Morgan, D.J.; Freakley, S.J.; Johnston, P.; Kiely, C.J.; Hutchings, G.J. Investigation of the Active Species in the Carbon-Supported Gold Catalyst for Acetylene Hydrochlorination. *Catal. Sci. Technol.* **2016**, *6*, 5144–5153. [CrossRef]

44. Malta, G.; Kondrat, S.A.; Freakley, S.J.; Davies, C.J.; Lu, L.; Dawson, S.; Thetford, A.; Gibson, E.K.; Morgan, D.J.; Jones, W.; et al. Identification of Single-Site Gold Catalysis in Acetylene Hydrochlorination. *Science* **2017**, *355*, 1399–1403. [CrossRef]

45. Yi, N.; Saltsburg, H.; Flytzani-Stephanopoulos, M. Hydrogen Production by Dehydrogenation of Formic Acid on Atomically Dispersed Gold on Ceria. *ChemSusChem* **2013**, *6*, 816–819. [CrossRef] [PubMed]

46. Wang, A.; Li, J.; Zhang, T. Heterogeneous Single-Atom Catalysis. *Nat. Rev. Chem.* **2018**, *2*, 65–81. [CrossRef]

47. Dhakshinamoorthy, A.; Primo, A.; Concepcion, P.; Alvaro, M.; Garcia, H. Doped Graphene as a Metal-Free Carbocatalyst for the Selective Aerobic Oxidation of Benzylic Hydrocarbons, Cyclooctane and Styrene. *Chem. A Eur. J.* **2013**, *19*, 7547–7554. [CrossRef]

48. Gao, Y.; Hu, G.; Zhong, J.; Shi, Z.; Zhu, Y.; Su, D.S.; Wang, J.; Bao, X.; Ma, D. Nitrogen-Doped sp2-Hybridized Carbon as a Superior Catalyst for Selective Oxidation. *Angew. Chem. Int. Ed.* **2013**, *52*, 2109–2113. [CrossRef] [PubMed]

49. Gupta, N.; Khavryuchenko, O.; Villa, A.; Su, D. Metal-Free Oxidation of Glycerol over Nitrogen-Containing Carbon Nanotubes. *ChemSusChem* **2017**, *10*, 3030–3034. [CrossRef]

50. Ciftci, A.; Ligthart, D.A.J.M.; Pastorino, P.; Hensen, E.J.M. Nanostructured Ceria Supported Pt and Au Catalysts for the Reactions of Ethanol and Formic Acid. *Appl. Catal. B Environ.* **2013**, *130–131*, 325–335. [CrossRef]

51. Bi, Q.Y.; Du, X.L.; Liu, Y.M.; Cao, Y.; He, H.Y.; Fan, K.N. Efficient Subnanometric Gold-Catalyzed Hydrogen Generation Via Formic Acid Decomposition under Ambient Conditions. *J. Am. Chem. Soc.* **2012**, *134*, 8926–8933. [CrossRef]

52. Rashid, T.; Kait, C.F.; Murugesan, T. Effect of Alkyl Chain Length on the Thermophysical Properties of Pyridinium Carboxylates. *Chin. J. Chem. Eng.* **2017**, *25*, 1266–1272. [CrossRef]

53. Schmidbaur, H.; Raubenheimer, H.G.; Dobrzanska, L. The Gold-Hydrogen Bond, Au-H, and the Hydrogen Bond to Gold, Au Center Dot Center Dot Center Dot H-X. *Chem. Soc. Rev.* **2014**, *43*, 345–380. [CrossRef]

54. Shlyakhova, E.V.; Bulusheva, L.G.; Kanygin, M.A.; Plyusnin, P.E.; Kovalenko, K.A.; Senkovskiy, B.V.; Okotrub, A.V. Synthesis of Nitrogen-Containing Porous Carbon Using Calcium Oxide Nanoparticles. *Phys. Status Solidi B* **2014**, *251*, 2607–2612. [CrossRef]

55. Ivanova, S.; Pitchon, V.; Zimmermann, Y.; Petit, C. Preparation of Alumina Supported Gold Catalysts: Influence of Washing Procedures, Mechanism of Particles Size Growth. *Appl. Catal. A Gen.* **2006**, *298*, 57–64. [CrossRef]

56. Perdew, J.P.; Burke, K.; Ernzerhof, M. Generalized Gradient Approximation Made Simple. *Phys. Rev. Lett.* **1996**, *77*, 3865. [CrossRef]

57. Goerigk, L.; Grimme, S. A Thorough Benchmark of Density Functional Methods for General Main Group Thermochemistry, Kinetics, and Noncovalent Interactions. *Phys. Chem. Chem. Phys.* **2011**, *11*, 6670–6688. [CrossRef]

58. Grimme, S.; Antony, J.; Ehrlich, S.; Krieg, H. A Consistent and Accurate Ab Initio Parametrization of Density Functional Dispersion Correction (DFT-D) for the 94 Elements H-Pu. *J. Chem. Phys.* **2010**, *132*, 154104. [CrossRef]